Available online at www.sciencedirect.com
ScienceDirect
Trans. Nonferrous Met. Soc. China 35(2025) 349−361
Transactions of Nonferrous Metals Society of China
www.tnmsc.cn

# Low-temperature pressureless consolidation of AlSi10Mg powders by low-intensity ultrasound

Yu-ze LI[1], Long-fei ZHU[1], Xin WANG[1], Song TANG[2], Ting LUO[3], Jian-yuan WANG[1]

1. School of Physical Science and Technology, Northwestern Polytechnical University, Xi'an 710100, China;
2. Herbert Gleiter Institute of Nanoscience, School of Materials Science and Engineering, Nanjing University of Science and Technology, Nanjing 210094, China;
3. State Key Laboratory of Solidification Processing, Northwestern Polytechnical University, Xi'an 710072, China

Received 29 June 2023; accepted 28 February 2024

**Abstract:** Low-intensity ultrasound was applied to the pressureless consolidation of AlSi10Mg powders in a broad temperature range from 600 to 860 °C. Under static conditions, the consolidation of AlSi10Mg powders can only be achieved at 860 °C, but still with the presence of some residual unconsolidated regions. The introduction of low-intensity ultrasound at this temperature eliminates the unconsolidated regions and transforms the columnar grains observed in original directional solidification into equiaxed or globular grains. Remarkably, the application of low-intensity ultrasound significantly reduces the consolidation temperature to 620 °C, without compromising the microhardness of the resulting samples when compared to static conditions. Furthermore, by lowering the temperature to 600 °C, a well-sintered porous material is obtained through the assistance of the low-intensity ultrasound.

**Key words:** low-intensity ultrasound; pressureless consolidation; aluminum powders; columnar-to-equiaxed transition; microhardness

## 1 Introduction

Powders metallurgy (PM) method is extensively employed in producing various metal and composite products, primarily because of its potential of near-net-shape manufacturing [1,2]. However, materials produced by PM process often suffer from inferior mechanical properties due to the residual porosity [3]. A number of advanced techniques have been developed to improve the performance of PM materials, including spark plasma sintering [4], thermo-mechanical consolidation [5], surface densification [6], and isostatic pressing [7]. Achieving highly dense materials often necessitates a cumbersome PM process, which is time- and energy-consuming [8,9]. For example, hot isostatic pressing requires to hold a high pressure at elevated temperature for up to 24 h [7,10]. Therefore, the goal of PM process is not only to achieve fully densified material, but also to enhance the processability of the material by simplifying the PM conditions, such as reducing the pressing forces, temperature and holding time. This requires continuous efforts to develop advanced methods to assist consolidation.

Recently, ultrasound has been found to be effective in various fields, including welding [11,12], surface treatment [13,14], casting [15,16], sintering [17,18] and others [19,20]. In the context of PM process, ultrasound can be applied in two stages: cold compaction [21] and hot pressing [22−28].

**Corresponding author:** Ting LUO, Tel: +86-18706850697, E-mail: t.luo@nwpu.edu.cn;
Jian-yuan WANG, Tel: +86-13474353420, E-mail: wangjy@nwpu.edu.cn
DOI: https://doi.org/10.1016/S1003-6326(24)66684-7

FARTASHVAND et al [21] applied ultrasound to the compaction of titanium powders, resulting in a 64% improvement in strength. CHEN et al [24] employed ultrasound in the hot pressing, fabricating nanocrystalline Ti-alloy with nearly full density. ABEDINI et al [26] incorporated ultrasound in the hot pressing of AA1100 powders, leading to significant improvement in density. KUMAR and PANDEY [27] found that the sintered density of Mg15Nb3Zn1Ca powders increased with the increase of the ultrasonic power. Several other researchers also applied ultrasound to the hot pressing for different materials and the main benefits include pore healing, higher density, enhanced strength [29−31], and so on.

Pressureless sintering is another important process in PM method, applied as a following process after cold compaction or an individual mode of PM method [32]. Ultrasound could also be employed to facilitate the sintering. WEI et al [30] found that the ultrasound efficiently lowers the reaction temperature between $Fe_2O_3$ and CaO to form $CaFe_2O_4$. SINGH and PANDEY [17] reported that the ultrasound optimized the distribution of the particles and reduced the porosity, thereby enhanced the density of the sintered copper components. Furthermore, ultrasound could also impact the solidification process of the remelting region during the sintering of the powders. The primary effects of ultrasound on the solidification process could be attributed to the cavitation and acoustic flow in the melt [33−35]. Under these contributions, the ultrasound-applied solidification process often leads to much finer grains.

Although ultrasound assistance has been demonstrated to have great potential in PM process, several challenges hinder its broader application. Firstly, the ultrasonic transformer rod must suffer from high pressure, high temperature, or both simultaneously, imposing stringent requirements on the ultrasonicator and the entire equipment. Secondly, elaborate horn is essential to realize the effective transmission of the vibration energy to the end of the horn [36]. Finally, during the pressureless PM process, transmitting the ultrasonic vibration to each particle is challenging due to the loose packing of the powders. Thus, high-intensity ultrasound is often necessary for the PM process. However, the limited ultrasonic power restricts its application on large-scale samples. Therefore, it is crucial to conduct fundamental investigations to understand the effect of the ultrasound on the sintering process of the loose-packed powders. The ultimate goal is to improve the properties while minimizing the energy consumption.

This study aims at facilitating the pressureless consolidation of the loose-packed powders by employing low-intensity ultrasound, and further reveals its impact on the microstructure and mechanical properties of AlSi10Mg. A low-intensity power ultrasound (20 kHz) was applied to the consolidation process of AlSi10Mg powders at different temperatures (600−860 °C). This study focuses on examining the transmission of the ultrasonic vibration to the powders and the effects of low-intensity ultrasound on the consolidation, microstructure evolution and mechanical properties of AlSi10Mg. The simplified process and equipment described in this study could technically reduce both the time and economic costs associated with the PM process and could be extendedly applied to various materials.

## 2 Experimental

### 2.1 Ultrasound-assisted consolidation experiment of AlSi10Mg powders

Pre-alloyed spherical powders with a nominal composition of Al−10Si−0.35Mg (in wt.%) were produced via a gas atomization method. The particle sizes of these powders are smaller than 50 μm in diameter and the mean size is approximately 35 μm. Ultrasound-assisted consolidation experiments of AlSi10Mg powders were conducted in an ultrasonic solidification equipment with the schematic diagram shown in Fig. 1.

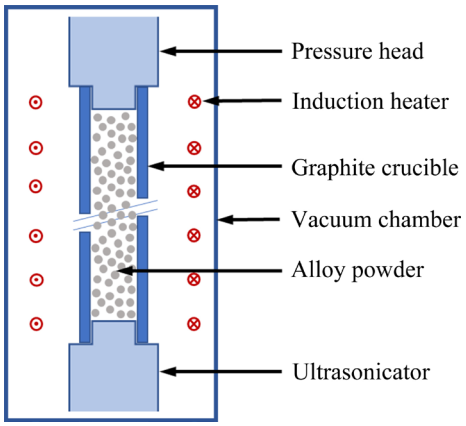


**Fig. 1** Schematic diagram of ultrasonic solidification equipment

A 15 g-batch of AlSi10Mg powders were tamped into a cylindrical graphite crucible measuring 10 mm in inner diameter and 140 mm in height. The experiments were conducted in a vacuum chamber filled with purified argon, maintaining a constant argon pressure throughout the procedure. A high-frequency induction coil was adopted to heat the sample and precise temperature control was achieved through a K-type thermo-couple connected to a thermal controller. A 45-steel rod was used to fasten the crucible on the top. Another 45-steel rod, connected to the ultrasonicator, was used to transmit ultrasound from the bottom of the crucible. As shown in Fig. 1, the bottom of the crucible was compacted tightly with the ultrasonicator rod, allowing ultrasound transmission from both the rod front and the crucible's sidewall. The applied ultrasound was maintained at a constant low intensity, with a longitudinal amplitude of only 4 μm at the top surface of the ultrasonicator rod.

To clarify the key impacts and the mechanism of the low-intensity ultrasound on the consolidation and the microstructure evolution during the PM process, three series of experiments were designed in the present study as follows.

(I) AlSi10Mg powders were heated to 860 °C and then held for 60 min. Afterwards, the heater was shut down and the temperature was then gradually decreased to the ambient temperature. This process is referred to as the free solidification. The experimental setup and the corresponding sample are abbreviated as EXP-860-FS and 860-FS, respectively.

(II) AlSi10Mg powders were heated to 660 °C or 860 °C and then held for 30 min. Afterwards, the crucible was pulled gradually from the heater to the cold zone at a velocity of 10 μm/s, leading to a temperature gradient of 15 °C/mm. This process is referred to as the directional solidification under static conditions. The experimental setup and these two samples are abbreviated as EXP-DS and 660-DS, 860-DS, respectively.

(III) AlSi10Mg powders were heated to various temperatures from 600 to 860 °C and then held for 15 min. Afterwards, ultrasound was employed and held for another 15 min. Finally, the crucible was pulled gradually to the cold zone, with the same pulling velocity and temperature gradient described in (II). Ultrasound was consistently applied throughout the entire duration of the experiment. This process characterized as the directional solidification under ultrasonic conditions. The experimental setup and these samples are abbreviated as EXP-DS-US and (600, 620, 640, 660, 860)-DS-US, respectively.

### 2.2 Characterization of raw powders and PM fabricated samples

The size distribution and the microstructure of the raw AlSi10Mg powders were first characterized by scanning electron microscopy (SEM, Verios G4). To quantitatively assess the applied ultrasound, transverse amplitudes at different positions of the crucible were measured using a KathMatic KV laser vibrometer during the experiment. The longitudinal amplitude of 4 μm at the top surface of the ultrasonicator rod was also detected by the same instrument. Specimens taken longitudinally along the central axis of the PM fabricated rod were prepared for microstructural examinations and microhardness tests. These specimens were ground to 2000# grit abrasive paper and then mechanically polished. The microstructures and compositions were examined and analyzed by optical microscopy (OM, Zeiss) and SEM (Verios G4). The differential scanning calorimetry (DSC) experiment was carried out using a Netzsch DSC 404C differential scanning calorimeter under pure argon gas condition, employing a scan rate of 10 °C/min for both the heating and cooling processes. Hardness tests were conducted using an automatic Vickers standard tester (load of 0.98 N for 15 s). To ensure the reliability of results, the hardness for each sample was tested from at least 5 random points and the indentation interval is at least 1 mm from each other.

## 3 Results

### 3.1 Characteristics of AlSi10Mg powders

Figure 2 shows the morphology and the microstructure of the AlSi10Mg powders using SEM. The majority of the powders exhibit a well-spherical shape with a smooth surface as shown in Fig. 2(a). The rapid solidification employed in the gas atomization method results in a homogenized microstructure within each particle and no bulk precipitates are observed, as depicted in Figs. 2(b, c). A fine microstructure is observed in

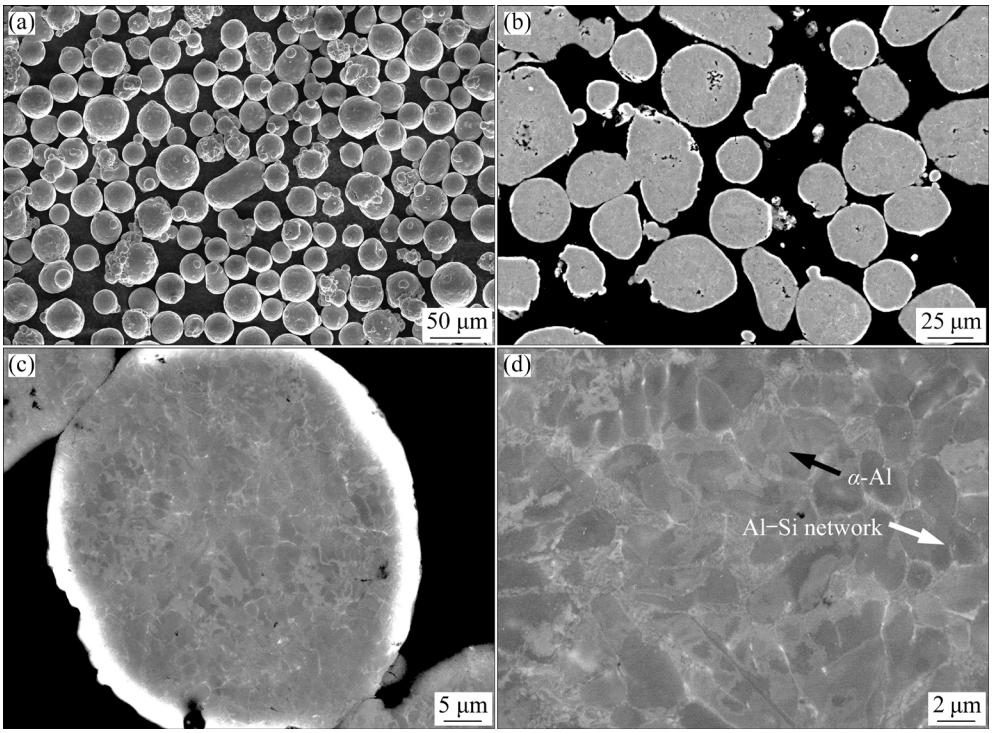


**Fig. 2** SEM images of AlSi10Mg powders: (a) Morphology of powders; (b) Cross-section microstructure of powders; (c, d) Magnified SEM images showing microstructure of $\alpha$-Al and eutectic Al−Si network

the AlSi10Mg powders, comprising of $\alpha$-Al phases (gray regions in Figs. 2(c, d), pointed out by the black arrow) and a nano-sized eutectic Al−Si network (bright regions in Figs. 2(c, d), pointed out by the white arrow).

Figure 3 shows the DSC profile of the AlSi10Mg raw powders with a heating rate of 10 °C/min. After reaching the maximum temperature of 700 °C, the sample was cooled down to room temperature with a cooling rate of 10 °C/min. The results show that the starting temperature of the phase transition is approximately 567 °C, whereas the remelting of the AlSi10Mg powders initiates. The phase transition is completed when the powders are fully remelted and the corresponding temperature is approximately 600 °C. Afterwards, the microstructure of the DSC-test sample was examined. Even though the powders were held at temperatures higher than the melting temperature of 567 °C for a duration longer than 25 min, the consolidation of the raw powders did not occur during the whole DSC experiment.

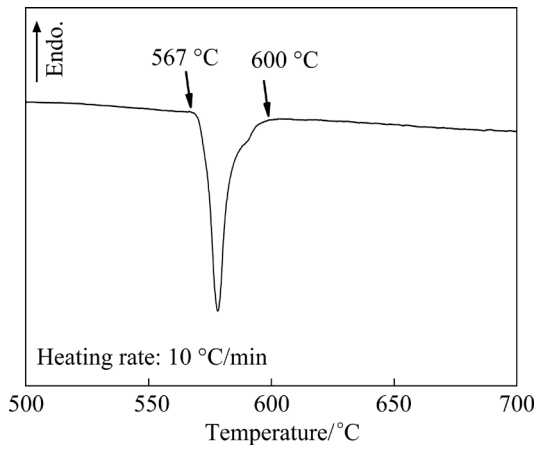


**Fig. 3** DSC profile of AlSi10Mg raw powders

### 3.2 Transverse amplitude curve of applied ultrasound

The transverse amplitudes were measured after the crucible was equipped and securely fastened into the experimental setup, as depicted in Fig. 1. The ultrasound, characterized by both longitudinal and transverse vibration, is describe in Fig. 4(a). For the transverse vibration tests, positions were along the same sideline of the crucible, staring from 1 mm from the bottom and moving upwards at an interval of 2 mm. The transverse amplitude curve of the crucible under experiment conditions is shown in Fig. 4(b). Error bars at the positions of 1 mm and 5 mm from the bottom are obscured by the symbols. The results indicate that the transverse vibration

amplitude of the crucible in this experimental setup is approximately 1 μm, albeit with fluctuations observed from the bottom to the top.

### 3.3 Microstructures of 860-FS sample

Figure 5 shows the microstructures of the 860-FS sample using OM. In most areas of 860-FS, the AlSi10Mg powders were well interfused and consolidated, forming large columnar dendrites (Fig. 5(a)) and small equiaxed dendrites (Fig. 5(b)) of primary $\alpha$-Al phases. However, some transition bands are noticeable, particularly at the edge of the fabricated rod, as indicated by the white circle in Fig. 5(c). These bands partition the overall region into smaller sections. Within these bands, porosities are evident, as denoted by the white arrow in Fig. 5(c). Figure 5(d) shows a magnified view of such a band, revealing the presence of micro-sized precipitates as indicated by the black arrows. In addition, the morphology of the raw particles could be discernible in this area, with the existence of the cracks between neighboring particles, as pointed out

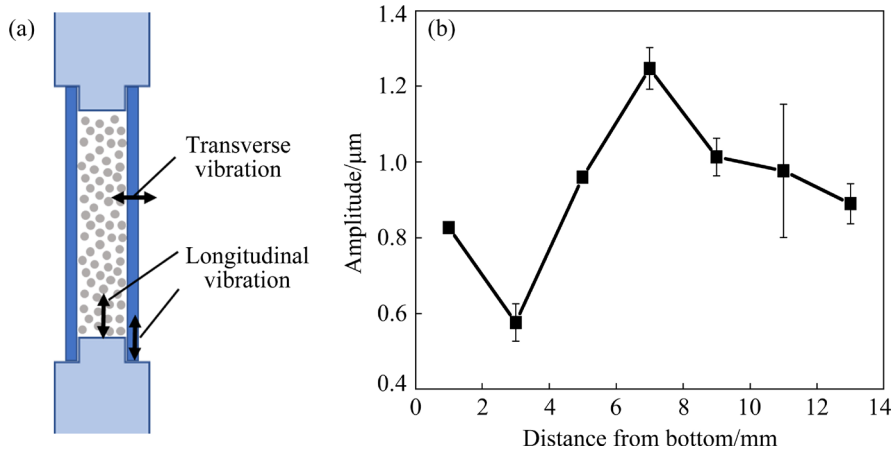


**Fig. 4** Schematic diagram showing ultrasonic vibration of crucible (a) and transverse vibration amplitude with distance from bottom to top of crucible (b)

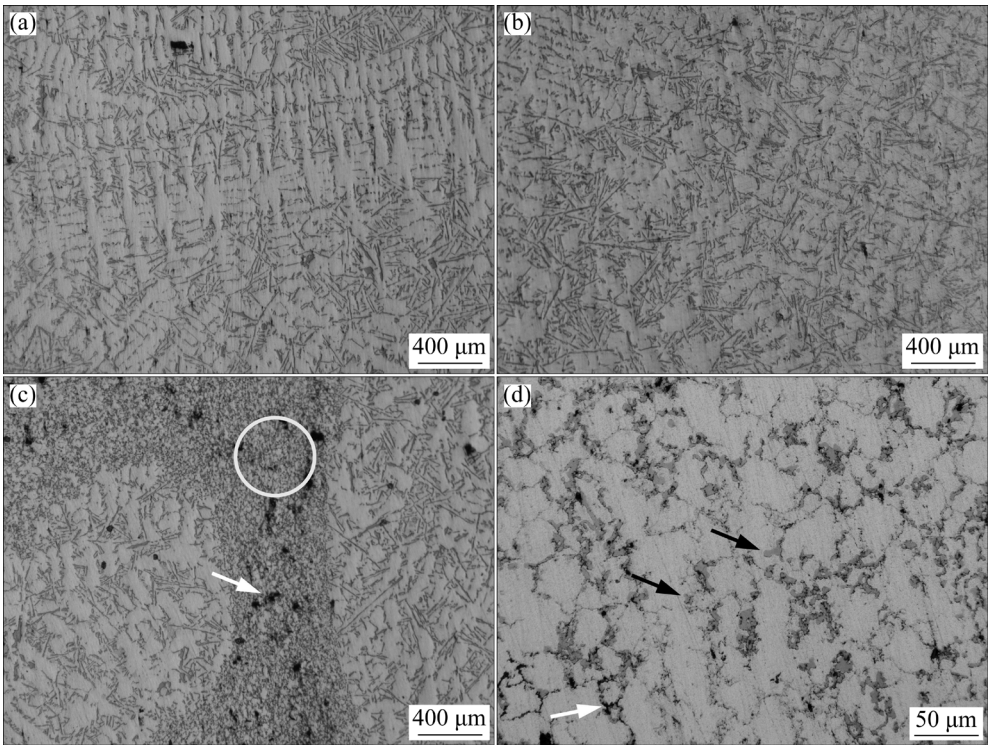


**Fig. 5** Microstructures of 860-FS sample using OM: (a, b) Large columnar dendrites and small equiaxed dendrites of primary $\alpha$-Al phases, respectively; (c, d) Microstructures at low-magnification and high-magnification showing inadequate consolidation bands, respectively

by the white arrow. This EXP-860-FS experiment demonstrates effective interfusion and consolidation of AlSi10Mg powders at 860 °C, but some inadequate consolidation regions are also present.

### 3.4 Microstructures of 860-DS and 860-DS-US samples

The microstructures of the 860-DS and 860-DS-US samples are shown in Figs. 6(a, c) and Figs. 6(b, d), respectively. The growth of the primary $\alpha$-Al phase could be observed in two distinct stages. In the bottom region of the sample under static conditions, corresponding to Stage I, the primary $\alpha$-Al phase grows as equiaxed dendrites (Fig. 6(c)). As the sample moves from the heat zone to the cold zone, the equiaxed to columnar transition (ECT) occurs (Fig. 6(a)), making a transition from Stage I to Stage II. At Stage II, the $\alpha$-Al phase displays as well-arranged large columnar dendrites, with some dendrites extending throughout the entire Stage II.

Upon the application of the ultrasound, the resulted primary $\alpha$-Al phase in Stage I is characterized by fine globular grains with an average size of 200 μm (Fig. 6(d)), which is nearly identical to the trunk diameter of the $\alpha$-Al dendrites in the same stage of 860-DS. The globular growth of the $\alpha$-Al phase gradually transforms into equiaxed morphology from Stage I to Stage II, as observed in the top region of the 860-DS-US sample (Fig. 6(b)). Notably, the diameter of the $\alpha$-Al dendrite trunk is visibly smaller than the value in the same stage of 860-DS (Fig. 6(a)).

### 3.5 Characteristics of samples fabricated at 600−660 °C

Figure 7 shows the macrostructures of the 660-DS, 600-DS-US and 660-DS-US samples. Under static conditions, the consolidation of the raw powders does not occur at 660 °C, as shown in Fig. 7(a). Once the ultrasound is employed, well-structured rods are produced both at 600 °C and 660 °C (Figs. 7(b, c)), albeit two insufficient consolidation regions at the top and the bottom of 600-DS-US are present (Fig. 7(b)). The total volume of the 600-DS-US is much larger than that of 660-DS-US, which could be concluded from the same diameter of the two but a much larger length of 600-DS-US. The volume of 600-DS-US is almost the same as that of the initially packed powders, while the volume of 660-DS-US is close to the complete densified value calculated by the mass of the fabricated AlSi10Mg alloy.

Figure 8 shows the microstructures of the (600, 620, 640, 660)-DS-US samples using OM. It can be seen that fully consolidated microstructures are

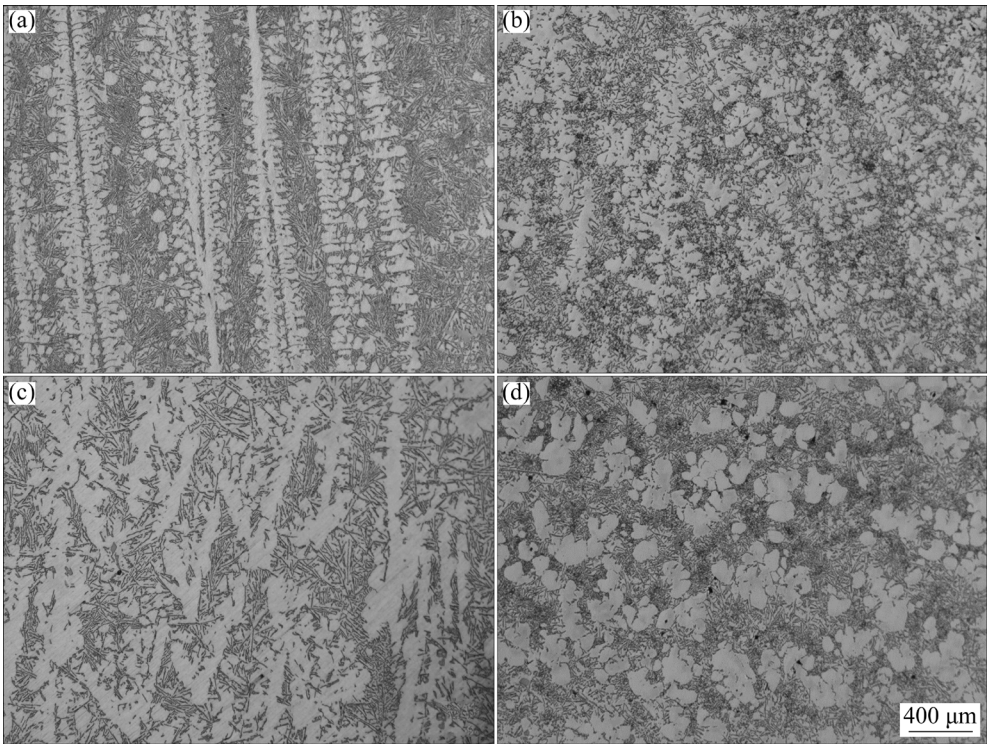


**Fig. 6** Microstructures of 860-DS (a, c) and 860-DS-US (b, d) samples at top (a, b) and bottom (c, d)

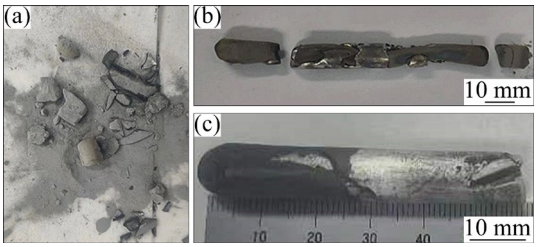


**Fig. 7** Macrostructures of different samples: (a) 660-DS; (b) 600-DS-US; (c) 660-DS-US

observed at all temperatures spanning from 660 to 620 °C under DS-US conditions. This demonstrates a remarkable improvement of the PM properties of AlSi10Mg powders due to the application of ultrasound, although the microstructural features vary among samples fabricated at different temperatures.

For the 660-DS-US sample, a large amount of primary $\alpha$-Al phase is evident, with discernible growth feature observed both in columnar and equiaxed dendrites (Figs. 8(a, c)). For the 640-DS-US sample, the microstructure primarily comprises the eutectic phase, accompanied with a small amount of dispersed $\alpha$-Al phase (Figs. 8(b, d)). For the 620-DS-US sample, the microstructure features exhibited in 660-DS-US and 640-DS-US are observed in different regions (Figs. 8(e, g)). When the heating temperature continuously decreases to 600 °C, the microstructure consists of metallurgical network interspersed with a large number of porosities (Fig. 8(f)). The microstructure in high-magnification (Fig. 8(h)) reveals that most of the particles are well sintered and bonded with neighboring ones, resulting in a solid porous structure of 600-DS-US, while the fully remelting and infusing do not occur during this PM process at 600 °C.

SEM was further employed to analyze the solid porous structure of 600-DS-US, and the results are shown in Fig. 9. Except for the porous structure, fine and dispersed precipitates are observed in this sample, exhibiting a brighter contrast in the backscattered electron (BSE) imaging mode (Figs. 9(a, b)). This is significantly distinct from the homogenized microstructure of the raw powders in Figs. 2(b, c). These precipitates are detected both inside and near the surfaces of the particles. Some precipitates even bulge to form bumps on the particle surface as shown in Fig. 9(c). The energy dispersive spectrometer (EDS) was used to analyze the composition of the matrix and precipitate, respectively. The average compositions in the selected positions in Fig. 9(d) are listed in Table 1. It is shown that, after the ultrasound-assisted PM process at 600 °C, the primary elements in the matrix (Point 1) are inclusively Al and Mg, while the dominant element in the precipitate (Point 2) is Si.

### 3.6 Microhardness of different samples

Figure 10 shows the microhardness of the samples fabricated by the ultrasound-assisted PM process at different consolidation temperatures. The hardness of the 860-FS sample, which was fabricated at 860 °C under static conditions, is approximate HV 57 and is indicated by a blue dash line in Fig. 10, as a comparison to the ultrasound-assisted samples. The hardness of the 600-DS-US sample is about HV 10, which is compatible with its porous structure. When the consolidation temperature increases to 620 °C, the microhardness significantly increases to approximately HV 56.5, equivalent to the hardness of the sample fabricated at 860 °C under static conditions. With increasing the consolidation temperature in the ultrasound-assisted PM process, the hardness slightly increases, reaching the highest hardness of approximately HV 60 for the 660-DS-US sample.

## 4 Discussion

### 4.1 Transmission of ultrasonic vibration

The ultrasound is commonly applied during the melt treatment process or semi-solid state to enhance the formability or modulate the microstructure of the final part, in which a continuous matter exists to transmit the ultrasonic vibration. As for the ultrasound-assisted PM process, the pressing process is normally exerted to facilitate the transmission of ultrasonic vibration among the powders. However, during the pressureless PM process, it is difficult to achieve the consolidation of the powders due to the insufficient contact and inter-diffusion among powders. Ultrasound could improve the PM sample properties only if it could be effectively transmitted into each powder. Particularly, if the vibration is solely transmitted through the ultrasonicator rod, a configuration often

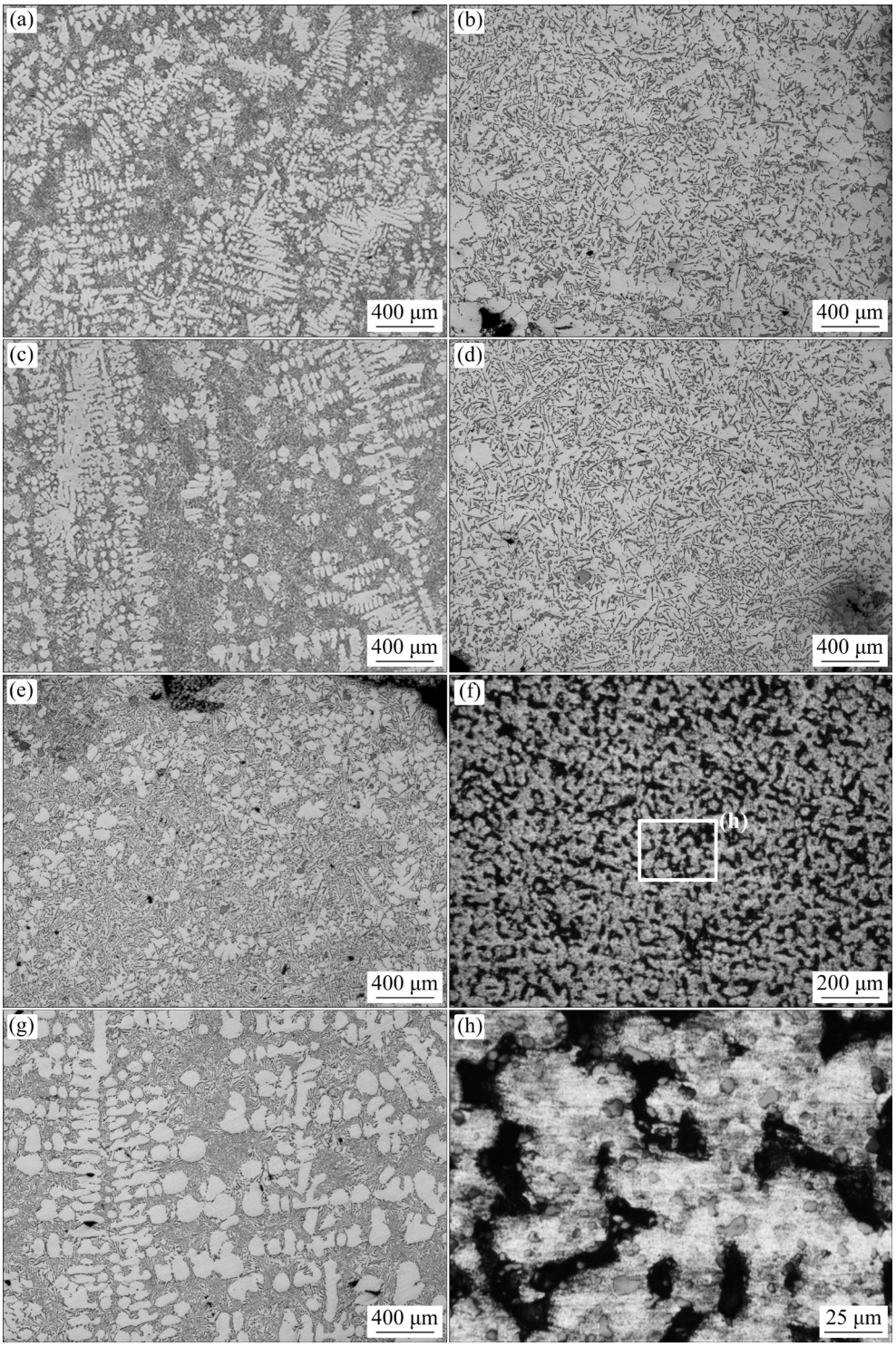


**Fig. 8** Microstructures of samples fabricated under DS-US conditions with heating temperatures from 600 to 660 °C: (a, c) Top and bottom regions of 660-DS-US, respectively; (b, d) Top and bottom regions of 640-DS-US, respectively; (e, g) Top and bottom regions of 620-DS-US, respectively; (f, h) Low-magnification and high-magnification of 600-DS-US, respectively

referred to as “single-source ultrasound”, which becomes challenging to generate adequate vibration in loose-packed powders. Thus, single-source ultrasound is typically used in the solidification process [37].

In this study, the combined longitudinal and transverse vibrations were introduced respectively through the top surface of the ultrasonicator rod and

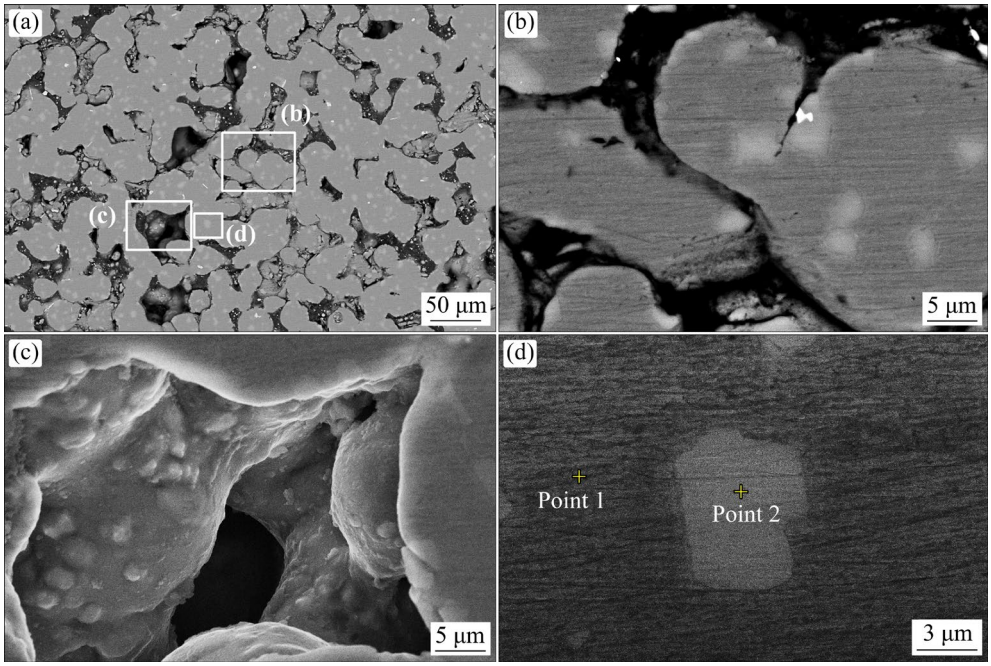


**Fig. 9** SEM image in low-magnification showing solid porous structure of 600-DS-US (a), one magnified region exhibiting presence of bright precipitates (b), precipitate bumps on powder surface viewed through one pore (c), and one precipitate within matrix with two crosses indicating EDS positions (d)

**Table 1** EDS chemical compositions of matrix and precipitate in 600-DS-US

| Sample | Content/at.% | | |
|---|---|---|---|
| | Mg | Al | Si |
| Matrix (Point 1 in Fig. 9(d)) | 0.17 | 99.83 | 0 |
| Precipitate (Point 2 in Fig. 9(d)) | 0.10 | 3.55 | 96.35 |

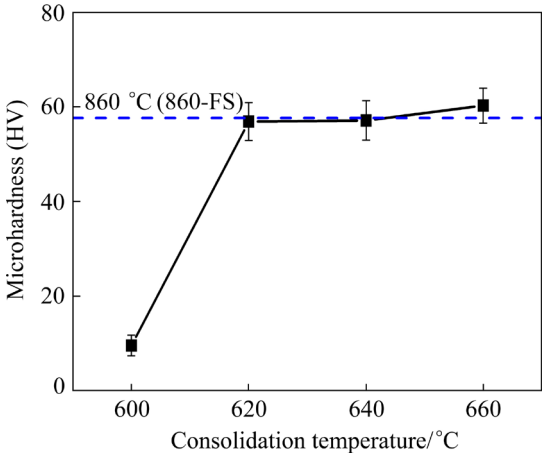


**Fig. 10** Microhardness of ultrasound-assisted samples as function of consolidation temperature

the sidewall of the crucible. Compared to single-source ultrasound, the double-source design and the dedicated mode developed in this work could lead to more effective transmission of the ultrasonic vibration into the loose-packed powders. A satisfactory consolidation of the AlSi10Mg powders was thus achieved by applying low-intensity ultrasound to the pressureless PM process. The consolidation temperature is lowered from 860 °C for the static condition to 620 °C for the ultrasound-assisted condition.

### 4.2 Ultrasound effect on PM process

In the pressureless PM process at elevated temperatures, the primary mechanisms underlying the consolidation of powders are diffusion along the particle−particle boundaries, remelting of the low-melting-point phase and infusion of the neighboring particles [32,38]. Theoretical liquidus and solidus temperatures under equilibrium conditions are respectively 596 and 577 °C for the AlSi10Mg alloy [39]. Consequently, complete remelting and adequate consolidation were anticipated for all the temperatures applied in this work. This assertion is further supported by the results of the DSC test, in which the temperature of the complete remelting of the AlSi10Mg powders is approximately 600 °C.

However, the consolidation of the raw powders did not take place at temperatures as high as 700 °C during the DSC process, or at 660 °C during the PM

process under static conditions. Even heated to 860 °C under static conditions, the 860-FS sample still exhibits some insufficient consolidation regions. This could be mainly attributed to the specific structure of the AlSi10Mg raw particles. As shown in Fig. 2(d), the microstructure of the AlSi10Mg particle is homogeneously composed of $\alpha$-Al phase and eutectic Al−Si network. When the powders are exposed to elevated temperatures, the eutectic phases will remelt primarily. Consequently, it necessitates a sufficient amount of time to attain complete remelting of the entire particle, particularly at lower temperatures as those applied in this work. In addition, a thin film of $Al_2O_3$, with a typical thickness of a few nanometers, forms on the surface of the Al alloy particle due to the oxidation activity of aluminum [40]. Under static conditions, this $Al_2O_3$ film effectively suppresses the inter-diffusion between particles, as well as the motion of the liquid phase generated in each particle at elevated temperatures, resulting in the formation of inadequate or unconsolidated regions under static conditions.

Figure 11 displays the schematic diagrams of the packing powders and their performance during the ultrasound-assisted PM process, in which the $Al_2O_3$ thin film is represented by the black regions. Ultrasound has two main beneficial effects on the AlSi10Mg powders during the PM process, i.e., friction and collision between powders, as indicated by the yellow and white arrows in Fig. 11(a), respectively. On the one hand, intensive friction and collision among powders generate a significant amount of heat, accelerating the inter-diffusion and remelting of the powders. On the other hand, the thin $Al_2O_3$ film on the scale of a few nanometers could be effectively broken by this friction and collision.

For a single particle, the network of the eutectic phase will remelt primarily when being exposed to elevated temperatures, as shown by the pink regions in Fig. 11(b). Upon the application of the ultrasonic vibration, the motion and merging of the liquid phases are enhanced greatly. The time required to achieve the entire remelting of the particle is thus shortened significantly. In addition, the thin $Al_2O_3$ film could also be broken by the ultrasonic vibration itself, which further accelerates the infusion of the neighboring particles. Under these conditions, when the temperature is appropriately adopted to enable the sufficient primary remelting, the infusion between powders is facilitated and accelerated effectively by the applying ultrasonic. The adequate consolidation structure is thus achieved, such as the PM samples fabricated at 620−860 °C under ultrasonic conditions.

However, as the applied temperature continues to decrease, such as to 600 °C in this work, the quantity of the liquid phase becomes insufficient to achieve complete remelting of the powders. Only part of the infusion between neighboring powders could take place, resulting in the porous structure of 600-DS-US. In addition, the ultrasonic vibration enhances the motion and merging of the liquid phases, along with the solute diffusion from the matrix to the liquid, as illustrated by the black arrows in Fig. 11(b). Therefore, during the following solidification of the liquid phases, large Si particles precipitate both inside and on the surface of the particles (Fig. 11(c)), which is evident in the microstructure shown in Fig. 9.

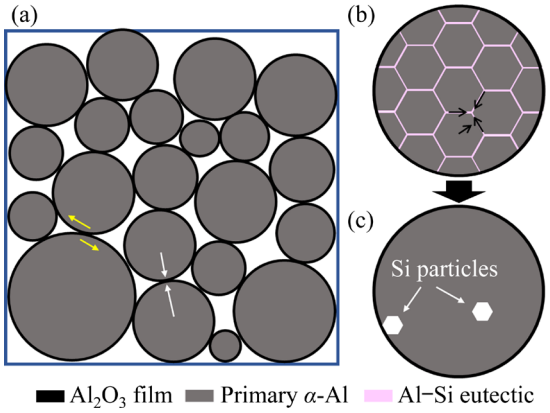


**Fig. 11** Schematic diagrams showing performance of powders during ultrasound-assisted PM process: (a) Packing of powders in crucible; (b) Primary remelting phases; (c) Precipitation of Si particles during PM process

### 4.3 Effect of ultrasound on evolution of solidified microstructure

Two main mechanisms underpin the beneficial effects of ultrasound on the solidification process, i.e., nucleation of new grains and fragmentation induced by cavitation, and homogenization by acoustic flow [33−35]. The cavitation introduced by the ultrasound not only improves the wetting behavior between the impurities and the alloy melt, but also generates local high undercooling, which

further stimulates heterogeneous nucleation. In addition, when ultrasound is applied in the growth process of the primary $\alpha$-Al phase, the cavitation-induced fragmentation occurs simultaneously. Due to the combining effects, the well-arrayed large columnar dendrites under the static condition transform into equiaxed dendrites or even globular grains. Furthermore, the acoustic flow helps to homogenize the temperature field, the solute field, as well as the flow field at the front of the solid−liquid interface, thus suppressing the inherent dominant growth orientation. Therefore, the crystals tend to grow isotopically and form equiaxed or even globular grains. The diameter of the $\alpha$-Al dendrites trunk is obviously decreased due to the shortened time for the dendrite growth.

When the ultrasound is applied at lower temperatures, such as at 620 or 640 °C in this work, only a small amount of primary $\alpha$-Al dendrites appear and the eutectic solidification microstructure is dominant. It is reasonable to believe that the cavitation-induced high undercooling plays an important role in enhancing the eutectic growth during the solidification process. However, the transformation from dendritic to eutectic solidification does not occur monotonously with decreasing the temperature under ultrasonic conditions. Dendritic growth is more pronounced at 620 °C compared to 640 °C. This could be attributed to many indeterminacies introduced during the pressureless PM process because of the loose packing of the powders and the temperature fluctuation triggered by the random friction and collision between the powders.

## 5 Conclusions

(1) The double-source ultrasound was effectively introduced into the consolidation process of AlSi10Mg powders. The longitudinal and transverse vibration was transmitted to the powders through the top surface of the ultrasonicator rod and the sidewall of the crucible, respectively.

(2) The consolidation of AlSi10Mg powders was only obtained at an elevated temperature of 860 °C under the static condition. With the application of ultrasound, the consolidation temperature of AlSi10Mg powders was decreased to 620 °C, mainly attributed to the friction and collision between the powders and the enhanced motion of the liquids inside and between the particles. A well-sintered porous material was obtained at 600 °C, with dispersed Si precipitates.

(3) In the ultrasound-assisted powder consolidation process, the non-consolidated regions were eliminated and the columnar structure was tuned to equiaxed or globular grains due to the ultrasound-induced cavitation and acoustic flow.

(4) Comparable microhardness of the PM materials was achieved under ultrasonic conditions while the consolidation temperature was decreased from 860 to 620 °C. The porous material fabricated at 600 °C exhibited high microhardness despite its significant porosities. This strategy offers new opportunities for pressureless powder densification at average or low temperatures by applying low-intensity ultrasound.

### CRediT authorship contribution statement

**Yu-ze LI:** Conceptualization, Methodology, Writing − Original draft; **Long-fei ZHU:** Investigation, Resources; **Xin WANG:** Visualization; **Song TANG:** Validation, Writing − Review & editing; **Ting LUO:** Formal analysis, Writing − Review & editing; **Jian-yuan WANG:** Supervision, Project administration.

### Declaration of competing interest

The authors declare that they have no known competing financial interests or personal relationships that could have appeared to influence the work reported in this paper.

### Acknowledgments

This work was supported by the National Natural Science Foundation of China (Nos. 52101051, 52130405, 51872241, 52101142), the Key Research Plan of Shaanxi Province, China (No. 2020ZDLGY13-03), the Key Research and Development Program of Shaanxi Province, China (No. 2023-YBGY-439), and the Fundamental Research Funds for the Central Universities, China (No. 5000210653).

### References

[1] KRUZHANOV V, ARNHOLD V. Energy consumption in powder metallurgical manufacturing [J]. Powder Metallurgy, 2012, 55(1): 14−21.

[2] LI Hui-zhong, CHE Yi-xuan, LIANG Xiao-peng, TAO hui, ZHANG Qiang, CHEN Fei-hu, HAN Shuo, LIU Bin.

Microstructure and high-temperature mechanical properties of near net shaped Ti−45Al−7Nb−0.3W alloy by hot isostatic pressing process [J]. Transactions of Nonferrous Metals Society of China, 2020, 30(11): 3006−3015.

[3] WONG-ÁNGEL W D, TÉLLEZ-JURADO L, CHÁVEZ-ALCALÁ J F, CHAVIRA-MARTÍNEZ E, VERDUZCO-CEDEÑO V F. Effect of copper on the mechanical properties of alloys formed by powder metallurgy [J]. Materials & Design, 2014, 58: 12−18.

[4] GAO Qiang, ZHANG Lai-qi, QIAO Yi, LI Jun-pin. Diffusion bonding behaviour of $\beta$−$\gamma$ TiAl alloys containing high niobium with Ti interlayer by spark plasma sintering [J]. Transactions of Nonferrous Metals Society of China, 2022, 32(12): 3973−3984.

[5] ZHAO Qin-yang, CHEN Yong-nan, XU Yi-ku, TORRENS R, BOLZONI L, YANG Fei. Cost-affordable and qualified powder metallurgy metastable beta titanium alloy by designing short-process consolidation and processing [J]. Materials & Design, 2021, 200: 109457.

[6] LI Xiao, GUO Biao, JIAN Jie, AO Jin-qing, TANG Qi-feng, SONG Jiu-peng, ZHANG Yu. A new surface vibration extrusion process for surface densification and improvement of properties in powder metallurgical steel [J]. Materials & Design, 2022, 216: 110514.

[7] XIAO Yi, LANG Li-hui, XU Wen-cai, ZHANG De-xin. Diffusion bonding of Ti−6Al−4V titanium alloy powder and solid by hot isostatic pressing [J]. Transactions of Nonferrous Metals Society of China, 2022, 32(11): 3587−3595.

[8] KOIZUMI M, NISHIHARA M. Isostatic processing: Techonology and application [M]. London: Elsevier Applied Science, 1991.

[9] YIN Jie, LI Yi-yu, WU Yi-quan. Near-net-shape processed ZnS ceramics by aqueous casting and pressureless sintering [J]. Ceramics International, 2016, 42(9): 11504−11508.

[10] DENG C F, WANG D Z, ZHANG X X, MA Y X. Damping characteristics of carbon nanotube reinforced aluminum composite [J]. Materials Letters, 2007, 61(14): 3229−3231.

[11] HUANG Zhi-yuan, FU Jia-nan, LI Xin, WEN Wen-xin, LIN Hong-ji, LOU Yan, LUO Feng, ZHANG Zhen-xuan, LIANG Xiong, MA Jiang. Ultrasonic-assisted rapid cold welding of bulk metallic glasses [J]. Science China: Materials, 2022, 65(1): 255−262.

[12] LEI Yu-cheng, WANG Zhi-wei, CHEN Xi-zhang. Effect of arc-ultrasound on microstructures and mechanical properties of plasma arc welded joints of $SiC_p$/Al MMCs [J]. Transactions of Nonferrous Metals Society of China, 2011, 21(2): 272−277.

[13] LIU Dan, LIU Dao-xin, GUAGLIANO M, XU Xing-chen, FAN Kai-fa, BAGHERIFARD S. Contribution of ultrasonic surface rolling process to the fatigue properties of TB8 alloy with body-centered cubic structure [J]. Journal of Materials Science & Technology, 2021, 61: 63−74.

[14] YIN Xiao-ming, LI Xun, LIU Yi-hang, GENG Da-xi, ZHANG De-yuan. Surface integrity and fatigue life of Inconel 718 by ultrasonic peening milling [J]. Journal of Materials Research and Technology, 2023, 22: 1392−1409.

[15] CHEN Mi, LIU Zhi-wei, JIA Yu-dong, YU Shen-wei, HE Yuan, ZHENG Bo-han. Effects of B element on microstructure and mechanical properties of $B_4C_p$/Al composites fabricated by ultrasound assisted casting method [J]. Transactions of Nonferrous Metals Society of China, 2023, 33(6): 1644−1654.

[16] WU Wen-hua, ZHAI Wei, ZHANG Yi-bao, XI Heng-dong, LIU Hai-man, ZHANG Jian, WEI Bing-bo. A comparative study of flow induced by 1D, 2D and 3D ultrasounds [J]. Science China: Technological Sciences, 2019, 62(07): 1224−1231.

[17] SINGH G, PANDEY P M. Ultrasonic assisted pressureless sintering for rapid manufacturing of complex copper components [J]. Materials Letters, 2019, 236: 276−280.

[18] YASUI K, HAMAMOTO K. Importance of dislocations in ultrasound-assisted sintering of silver nanoparticles [J]. Journal of Applied Physics, 2021, 130(19): 194901.

[19] ZHAI Wei, HUI Xi-dong, XIAO Ying, QIAO Ji-chao, WEI Shao-lou, WANG Tuo, NIE Li-hui, WEI Bing-bo. Structural rejuvenation and toughening of bulk metallic glass via ultrasound excitation technique [J]. Science China Technological Sciences, 2020, 63(11): 2395−2402.

[20] LI Qi, XIE Feng, CHANG Yong-feng, WANG Wei, ZHANG Li-bo. Behavior and mechanism of cyanide loss in ultrasound-assisted gold leaching process [J]. Transactions of Nonferrous Metals Society of China, 2023, 33(2): 609−618.

[21] FARTASHVAND V, ABEDINI R, ABDULLAH A. Influence of ultrasonic vibrations on the properties of press-and-sintered titanium [J]. Proceedings of the Institution of Mechanical Engineers, Part B: Journal of Engineering Manufacture, 2022, 236(11): 1518−1525.

[22] ABEDINI R, ABDULLAH A, ALIZADEH Y. Ultrasonic hot powder compaction of Ti−6Al−4V [J]. Ultrasonics Sonochemistry, 2017, 37: 640−647.

[23] LV Ke-zhen, YANG Kun, ZHOU Bo, ZHANG Feng, GUO Jing, HAN Chao, TIAN Yong. The densification and mechanical behaviors of large-diameter polymer-bonded explosives processed by ultrasonic-assisted powder compaction [J]. Materials & Design, 2021, 207: 109872.

[24] CHEN P, LIAO W B, LIU L H, LUO F, WU X Y, LI P J, YANG C, YAN M, LIU Y, ZHANG L C, LIU Z Y. Ultrafast consolidation of bulk nanocrystalline titanium alloy through ultrasonic vibration [J]. Scientific Reports, 2018, 8(1): 801.

[25] WARD A A, HARELAND C A, PALMERIO N E, CORDERO Z C. Thermally activated jamming in ultrasonic powder compaction [J]. Advanced Engineering Materials, 2021, 23(1): 2001019.

[26] ABEDINI R, ABDULLAH A, ALIZADEH Y. Ultrasonic assisted hot metal powder compaction [J]. Ultrasonics Sonochemistry, 2017, 38: 704−710.

[27] KUMAR A, PANDEY P M. Effect of ultrasonic assisted sintering on mechanical properties and degradation behaviour of Mg15Nb3Zn1Ca biomaterial [J]. Journal of Magnesium and Alloys, 2021, 9(6): 1989−2008.

[28] ABEDINI R, FARTASHVAND V, ABDULLAH A, ALIZADEH Y. Evaluation of process parameters and ultrasonic vibration in hot pressing of metal powders [J]. Materials Science and Engineering: B, 2022, 281: 115731.

[29] DEKHTYAR A I, MORDYUK B N, SAVVAKIN D G, BONDARCHUK V I, MOISEEVA I V, KHRIPTA N I. Enhanced fatigue behavior of powder metallurgy Ti−6Al−4V alloy by applying ultrasonic impact treatment [J]. Materials

Science and Engineering: A, 2015, 641: 348−359.
[30] WEI Rui-rui, LV Xue-wei, YANG Ming-rui, XU Jian. Effect of ultrasonic vibration treatment on solid-state reactions between $Fe_2O_3$ and CaO [J]. Ultrasonics Sonochemistry, 2017, 38: 281−288.
[31] FENG Bin, ZHOU Yao, PENG Cheng, LI Xiao-yan, LIU Ju-ying, WANG Yu-mei, RAO Ping-gen, WU Jian-qing. Vibration assisted hot-press sintering of AlN ceramics [J]. Journal of the American Ceramic Society, 2015, 98(6): 1711−1713.
[32] KAFKASLIOĞLU B, TÜR Y K. Pressureless sintering of $Al_2O_3$/Ni nanocomposites produced by heterogeneous precipitation method with varying nickel contents [J]. International Journal of Refractory Metals and Hard Materials, 2016, 57: 139−144.
[33] WANG J Y, WANG B J, HUANG L F. Structural evolution of Al−8%Si hypoeutectic alloy by ultrasonic processing [J]. Journal of Materials Science & Technology, 2017, 33(11): 1235−1239.
[34] SANDER J R G, ZEIGER B W, SUSLICK K S. Sonocrystallization and sonofragmentation [J]. Ultrasonics Sonochemistry, 2014, 21(6): 1908−1915.
[35] ZHAI W, LIU H M, HONG Z Y, XIE W J, WEI B. A numerical simulation of acoustic field within liquids subject to three orthogonal ultrasounds [J]. Ultrasonics Sonochemistry, 2017, 34: 130−135.
[36] SATPATHY M P, SAHOO S K, DATTA S. Acoustic horn design and effects of process parameters on properties of dissimilar ultrasonic welding aluminum to brass [J]. Materials and Manufacturing Processes, 2016, 31(3): 283−290.
[37] BALASUBRAMANI N, VENEZUELA J, YANG N, WANG G, STJOHN D, DARGUSCH M. An overview and critical assessment of the mechanisms of microstructural refinement during ultrasonic solidification of metals [J]. Ultrasonics Sonochemistry, 2022, 89: 106151.
[38] KOO B U, YI Y, LEE M, KIM B. Effects of particle size and forming pressure on pore properties of Fe−Cr−Al porous metal by pressureless sintering [J]. Metals and Materials International, 2017, 23(2): 336−340.
[39] MURRAY J L, MCALISTER A J. The Al−Si (aluminum-silicon) system [J]. Bulletin of Alloy Phase Diagrams, 1984, 5(1): 74−84.
[40] BRUCK H A, SHABANA Y M, XU B L, LASKIS J. Evolution of elastic mechanical properties during pressureless sintering of powder-processed metals and ceramics [J]. Journal of Materials Science, 2007, 42(18): 7708−7715.

# 低强度超声辅助实现 AlSi10Mg 粉末的低温无压固结

李玉泽[1]，朱龙飞[1]，王 昕[1]，唐 颂[2]，罗 婷[3]，王建元[1]

1. 西北工业大学 物理科学与技术学院，西安 710100；
2. 南京理工大学 材料科学与工程学院 格莱特研究院，南京 210094；
3. 西北工业大学 凝固技术国家重点实验室，西安 710072

**摘 要：**将低强度超声应用于 AlSi10Mg 粉末在 600~860 ℃宽温度范围的无压固结过程。在静态条件下，AlSi10Mg 粉末只能在高温 860 ℃时实现固结，但仍存在未固结区域。在此温度下施加低强度超声波消除了未固结区域，并将原始定向凝固条件下的柱状晶粒优转为等轴或球状晶粒。施加低强度超声将 AlSi10Mg 粉末的固结温度降低至 620 ℃，且获得了静态条件下高温固结样品同等级别的硬度。另外，施加低强度超声实现了 AlSi10Mg 粉末在 600 ℃下的烧结，获得了固结良好的多孔结构。

**关键词：**低强度超声；无压固结；铝基粉末；柱状晶−等轴晶转变；显微硬度

**(Edited by Wei-ping CHEN)**